1.4G:
Investigate Combustion in Premixed Charge Spark/Compression Ignition Engines

LDA Measurement of Gas Flow in a 4-stroke Motored Engine

Tomio OBOKATA, Tsuneaki ISHIMA and Hirohito YOKOTA
Graduate School of Mechanical Engineering,
Gunma University
1-5-1 Tenjin, Kiryu 376-8515, JAPAN

JECC: Japan National Committee on Energy Conservation in Combustion

JSME-RC226: Research committee on "International Cooperation for Active Combustion Control Technology by Synthesis of Advanced Measurements and Numerical Analysis"

Engine WG: Cooperative Research Work for In-Cylinder Flow Analysis

- An experimental study on in-cylinder flow measurement has been performed in order to make standard database for verifying numerical simulation.
- A laser Doppler anemometer (LDA) is applied to measure the velocities of vertical- and swirl-directions in the transparent sapphire cylinder of test engine made by Subaru.
- The time-series velocity data are readjusted by the ensemble averaged method using crank angle windows.
- Mean velocity and rms velocity are calculated with each crank angle.
- The tumble motion is evaluated by mean velocity map.

WG: Unsteady Flow in the Cylinder

- **Universities:**
  Chiba University, Gunma University,
  Hokkaido University, Okayama University

- **Car and Parts Industries**
  Honda R&D, Toyota Labs., Subaru-Fhi,
  Hitachi Nissan, Kawasaki, Mitsubishi Electric. co,
  Mitsubishi-Fuso, Yamaha-Motor co.,
  Toyota Suzuki

- **Software companies**
  Fluent, CDAJ

Objective

It is essential to control the gas flow in cylinder for improving the combustion in I.C. Engine

CFD of gas flow in cylinder is not easy because the flow is high speed, highly turbulent and complex.

To accumulate the standard data for verifying the CFD results, detailed gas velocities in the transparency cylinder of I.C. engine are measured by an LDA.

Test Engine

Engine specifications

Engine type	4-stroke, Single cylinder
Combustion chamber	Pentroof type
Bore × Stroke	96.9 mm×74 mm
Displacement	545.7 □□
Compression ratio	11.5
Intake valve opening	4 deg.
Intake valve closure	240 deg.
Exhaust valve opening	485 deg.
Exhaust valve closure	5 deg.

Operating condition

Motoring	600rpm
WOT	With TGV / Without TGV

Optical System

Specifications of LDV

Wavelength	632.8 nm
Beam separation	50 mm
Beam diameter	1.35 mm
Focal length	300 mm
Full beam angle	9.52°
Calibration factor	3.81 m/ s/ MHz
Mean diameter of waist	179 μ m
Measuring volume length	2.26 mm
Measuring volume width	179 μ m
Shift freaquancy	10 MHz

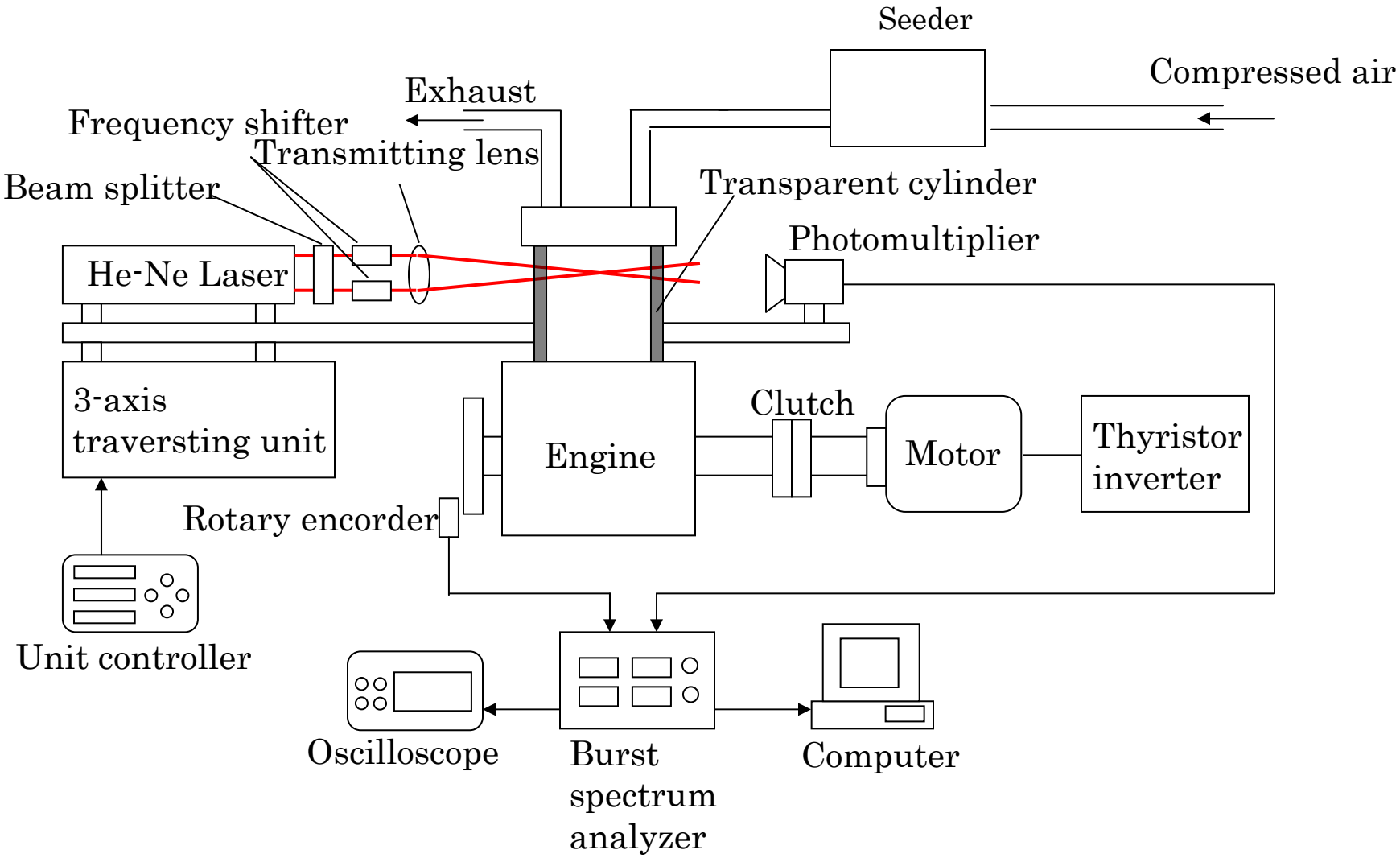

Layout of the experimental setup

Coordinate System and Measuring Points

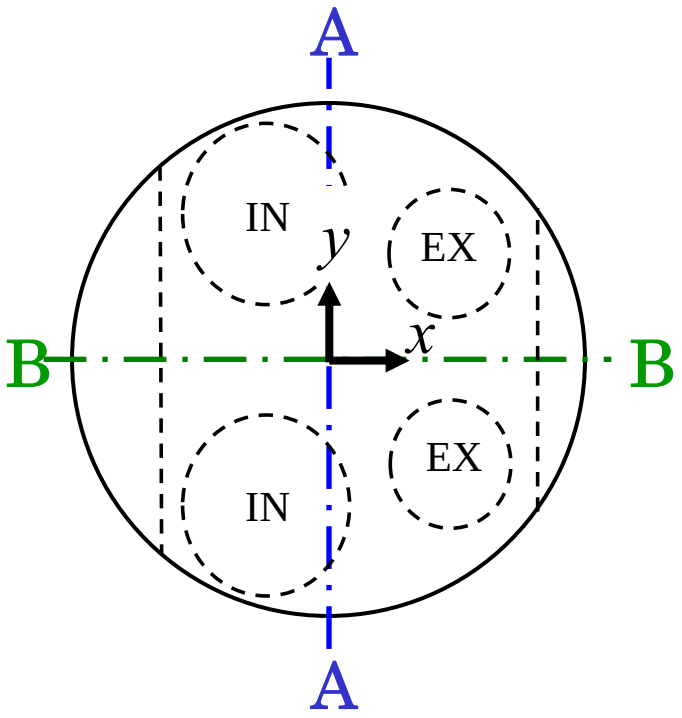

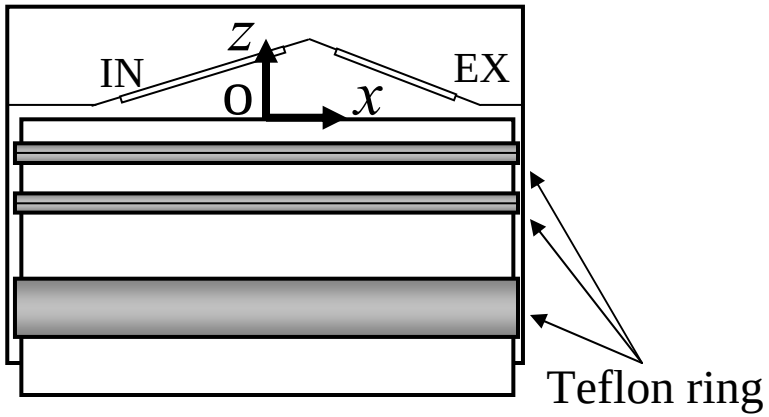

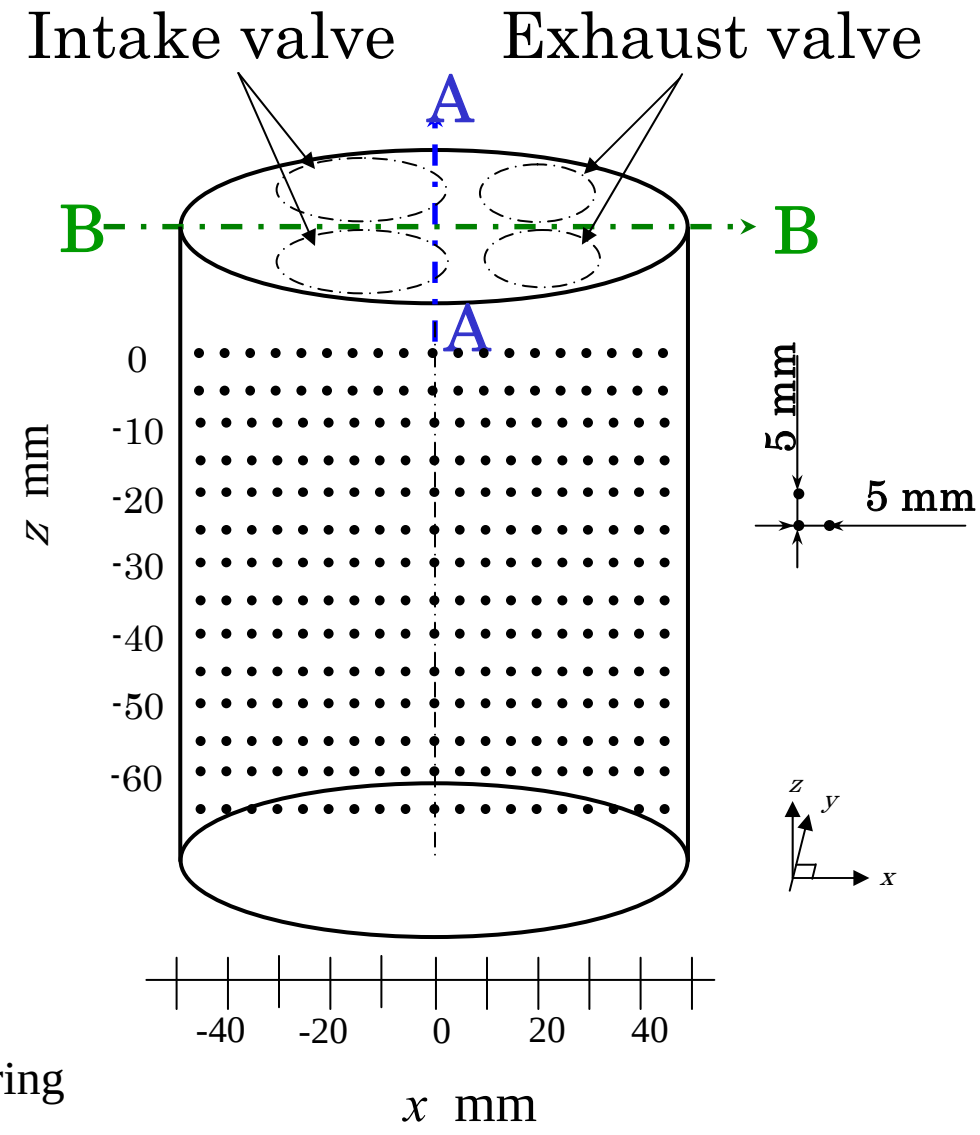

Measured velocity, Ensemble Averaged Mean Velocity and Fluctuating Intensity

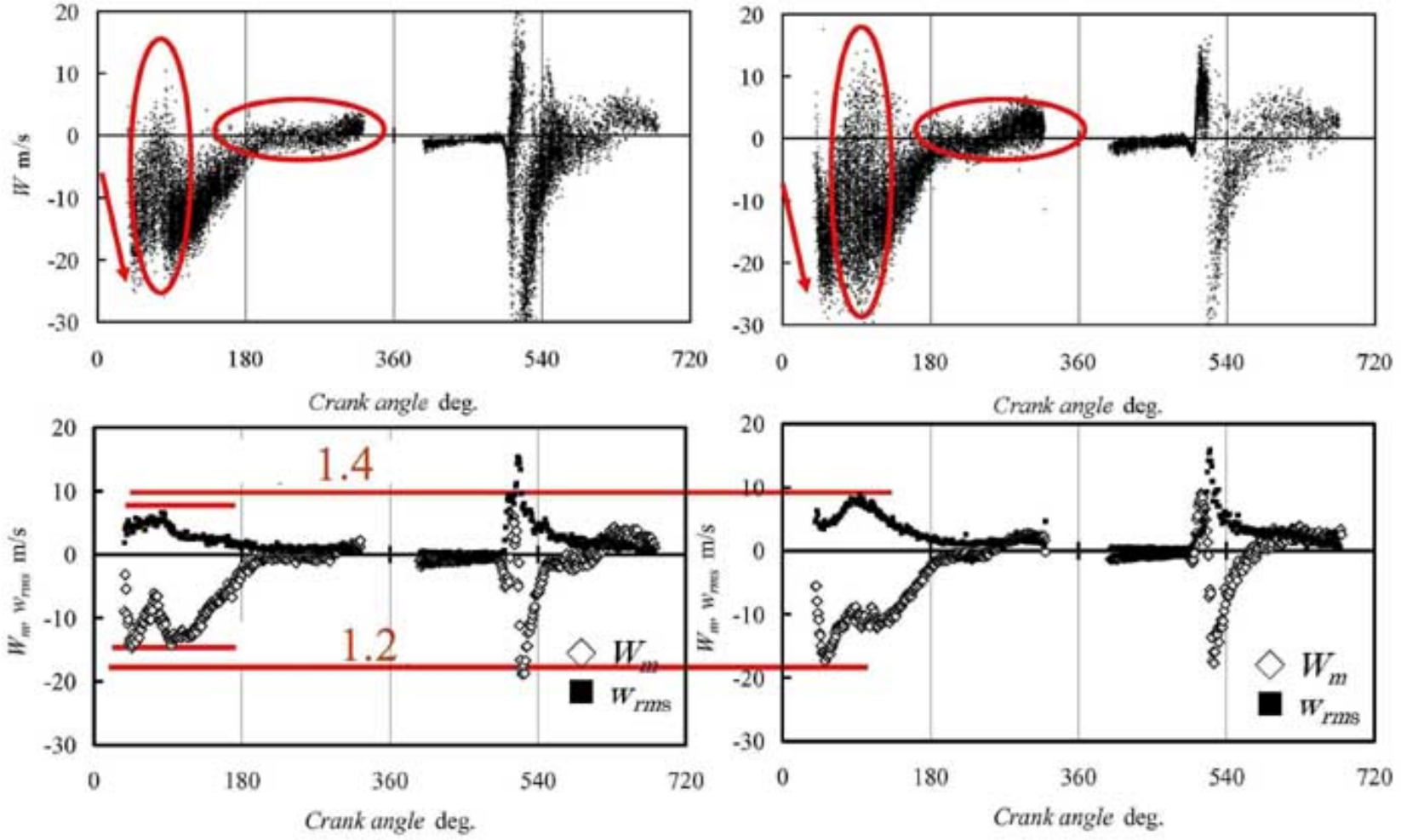

Without TGV

With TGV

Examples of axial velocity data (x,y,z = 0,0,-10mm)

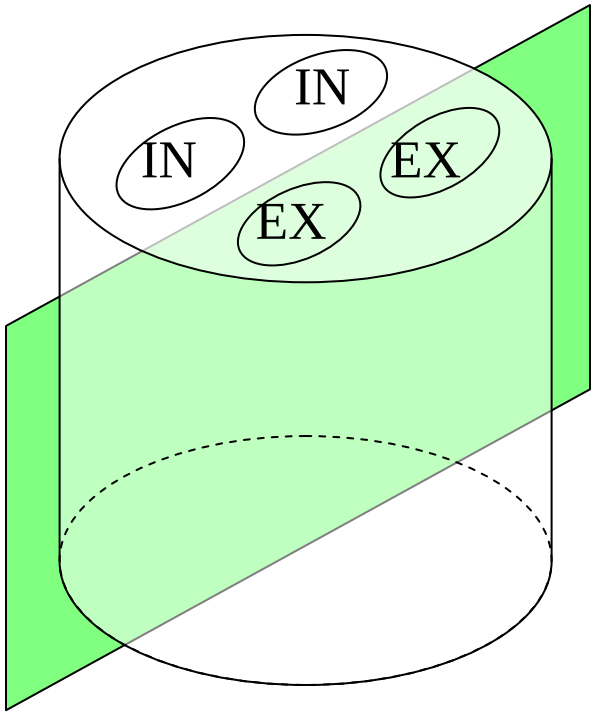

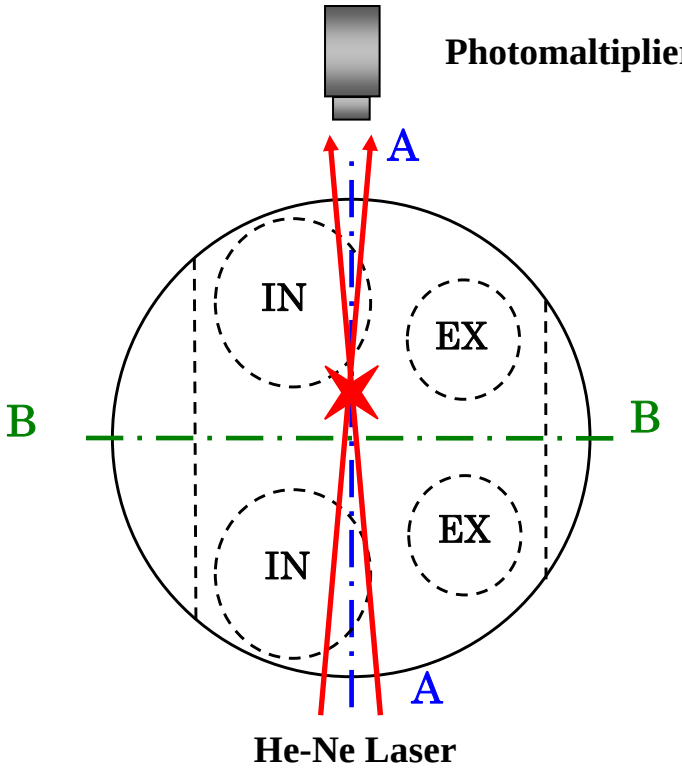

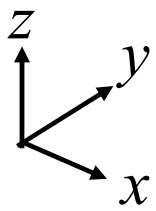

A-A

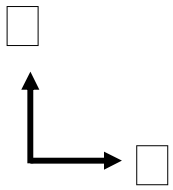

A-A Section

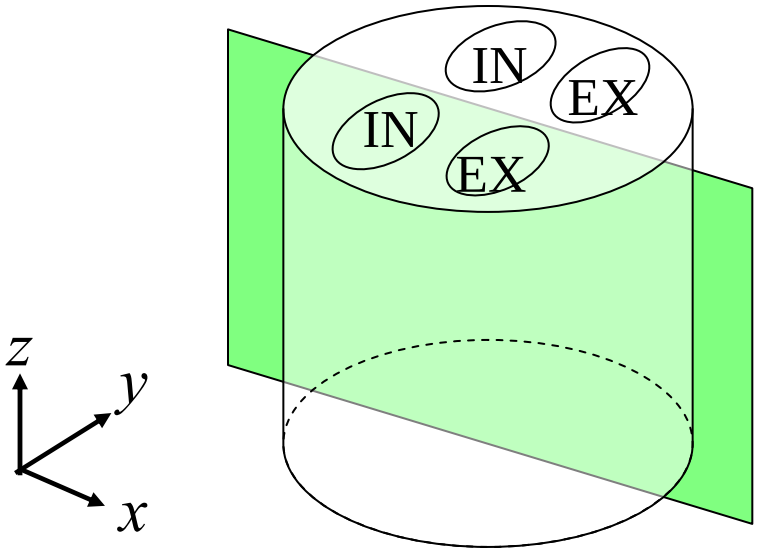
IN
EX
IN
EX
z
y
x

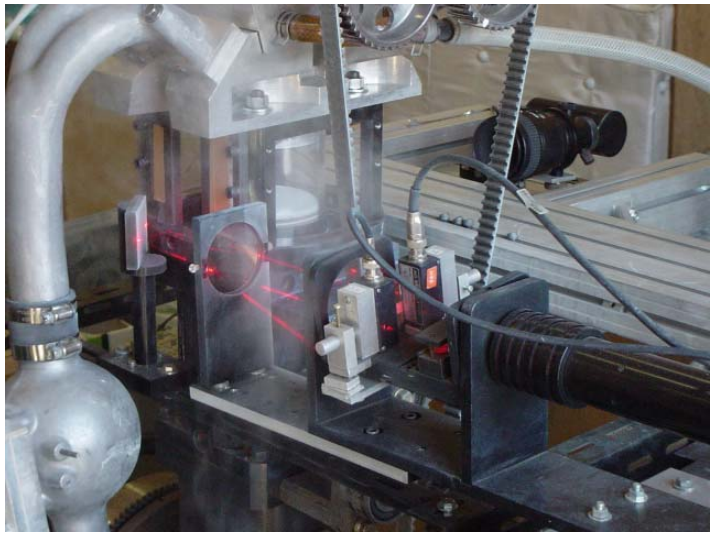

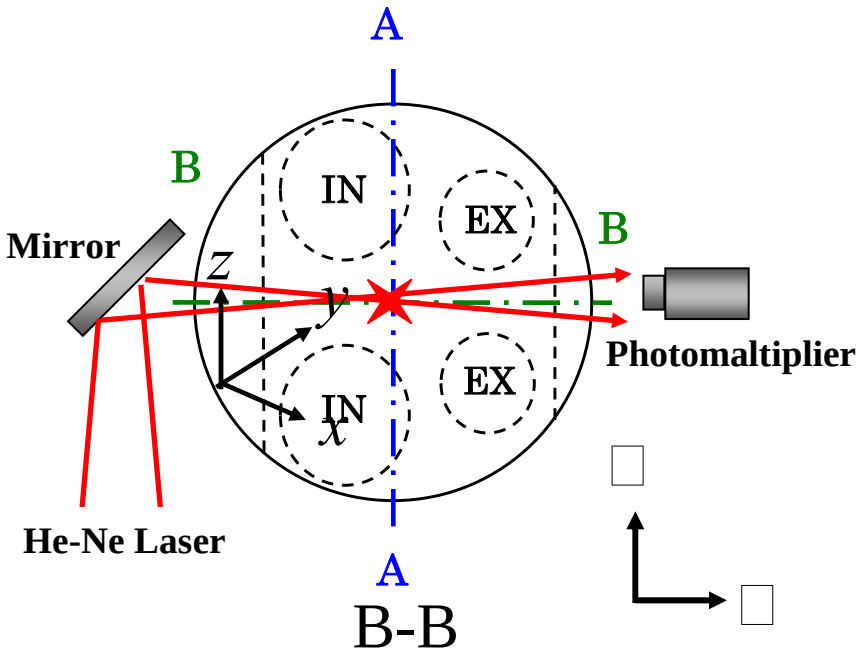
A
B
IN
EX
B
Mirror
z
y
Photomaltiplier
EX
IN
x
He-Ne Laser
A
B-B

B-B Section

Axial velocity in the Cylinder

Non-dimensional expression is used for velocities divided by the mean velocity of piston Up=1.48m/s

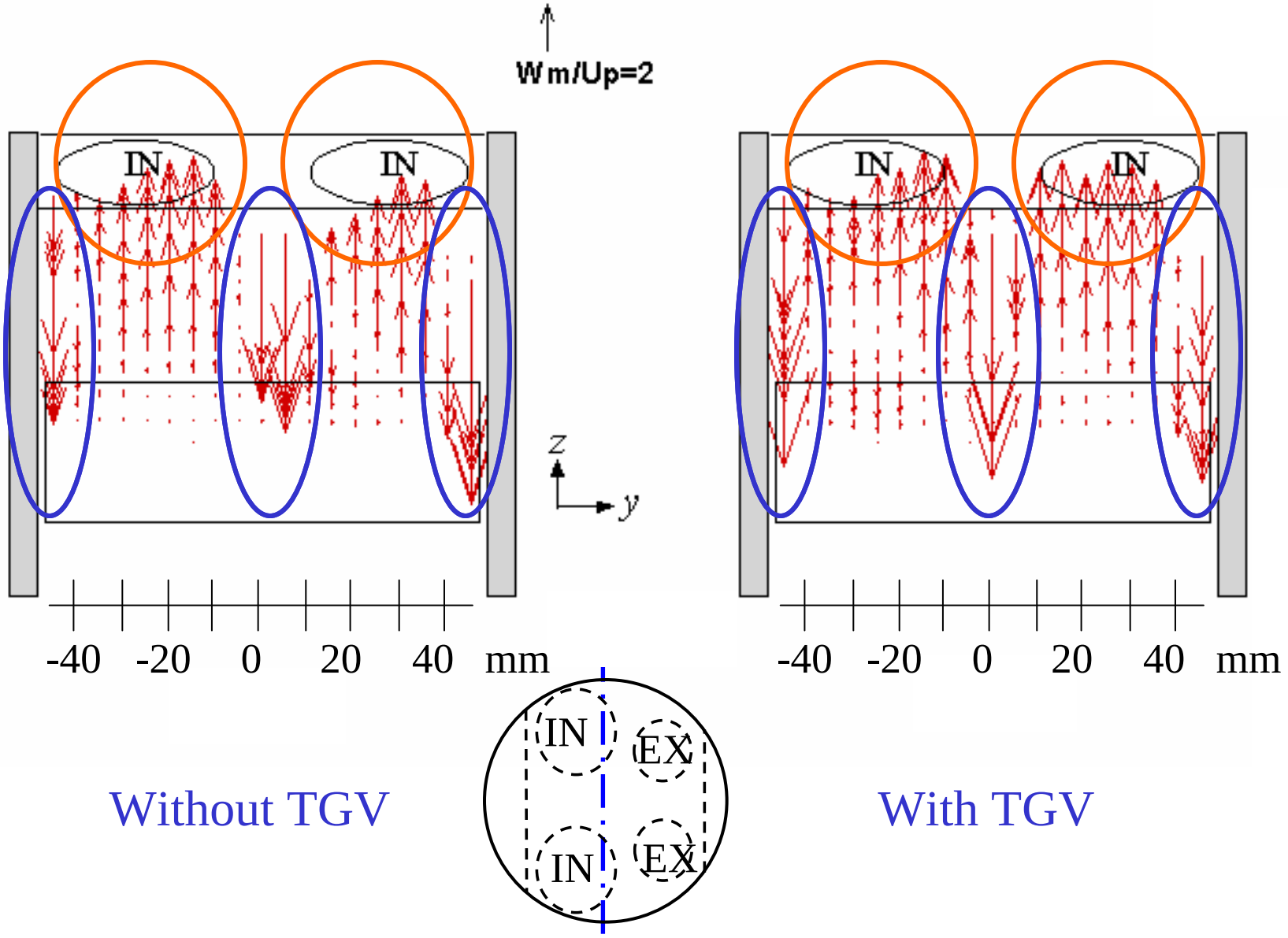

Ensembled-avereged mean velocity distributions of W_m at vertical section(A-A section at 90deg.)

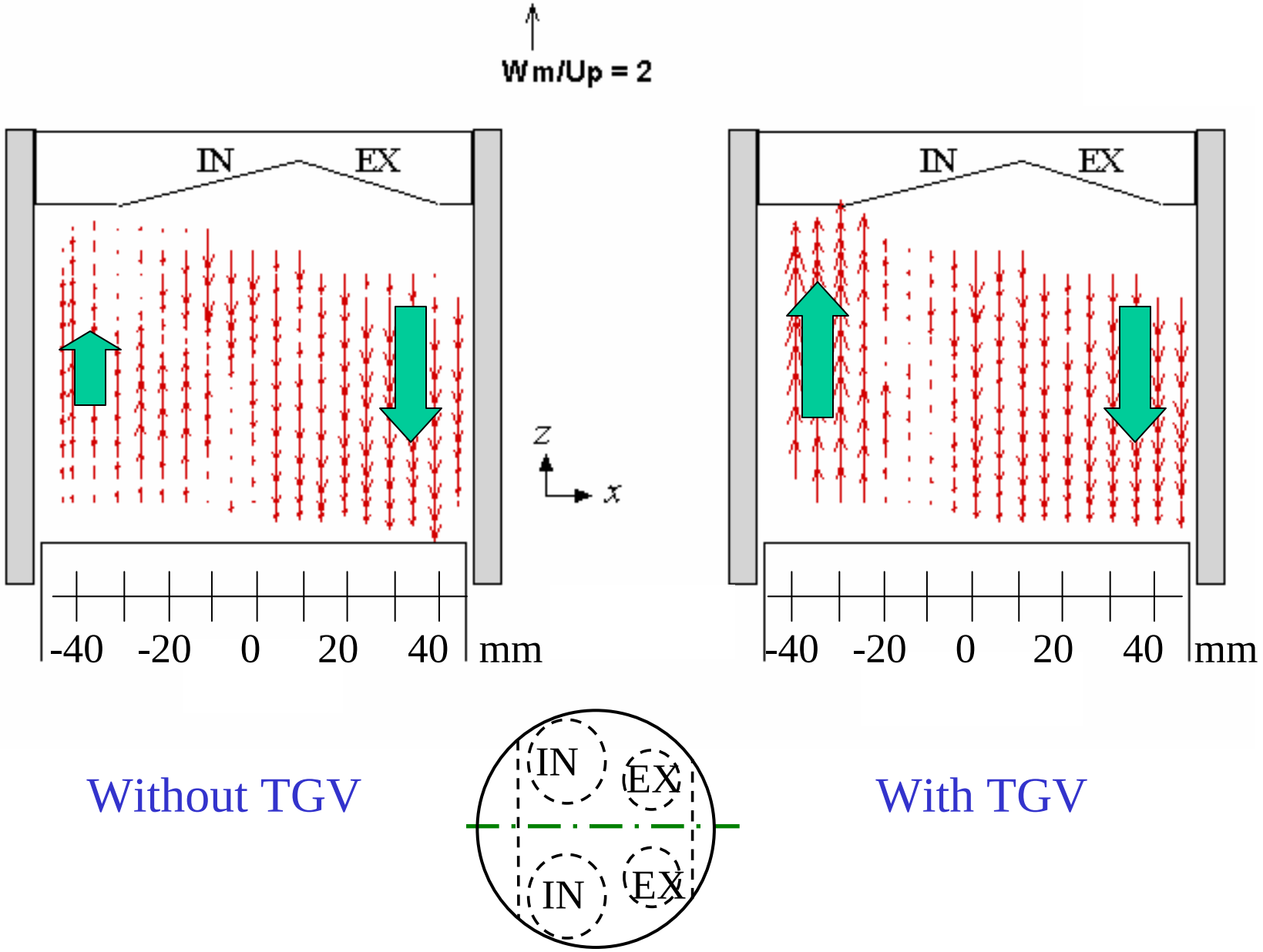

Ensembled-avereged mean velocity distributions of W_m at vertical section (B-B section at 180deg.)

Circumferential velocity in the cylinder

Non-dimensional expression is used for velocities divided by the mean velocity of piston Up=1.48m/s

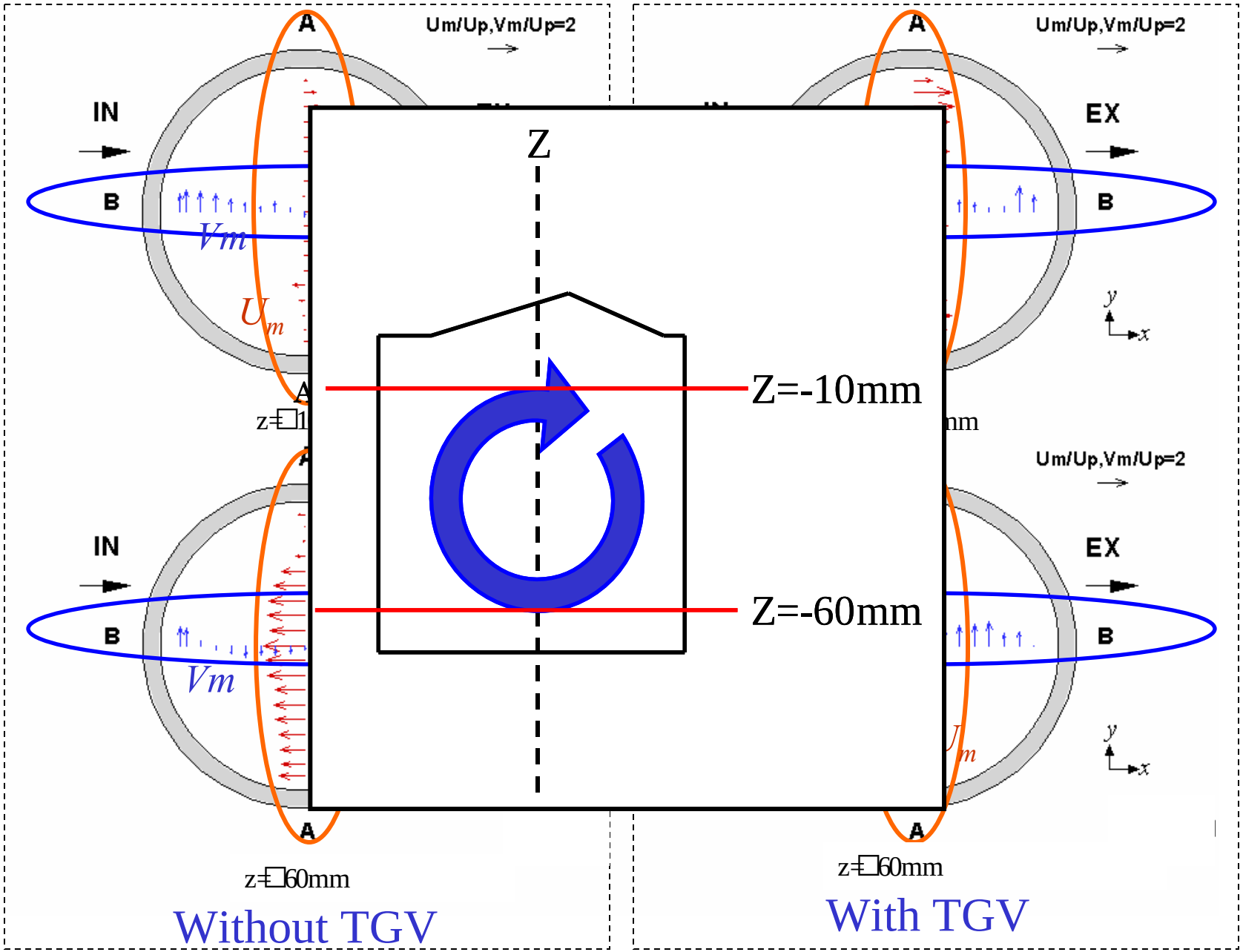

Ensembled-avereged mean velocity distributions of U_m and $V_m$at transversal section at 180deg.

Tumble Ratio

Simple evaluation

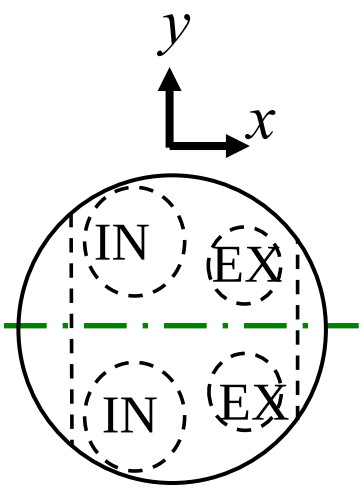

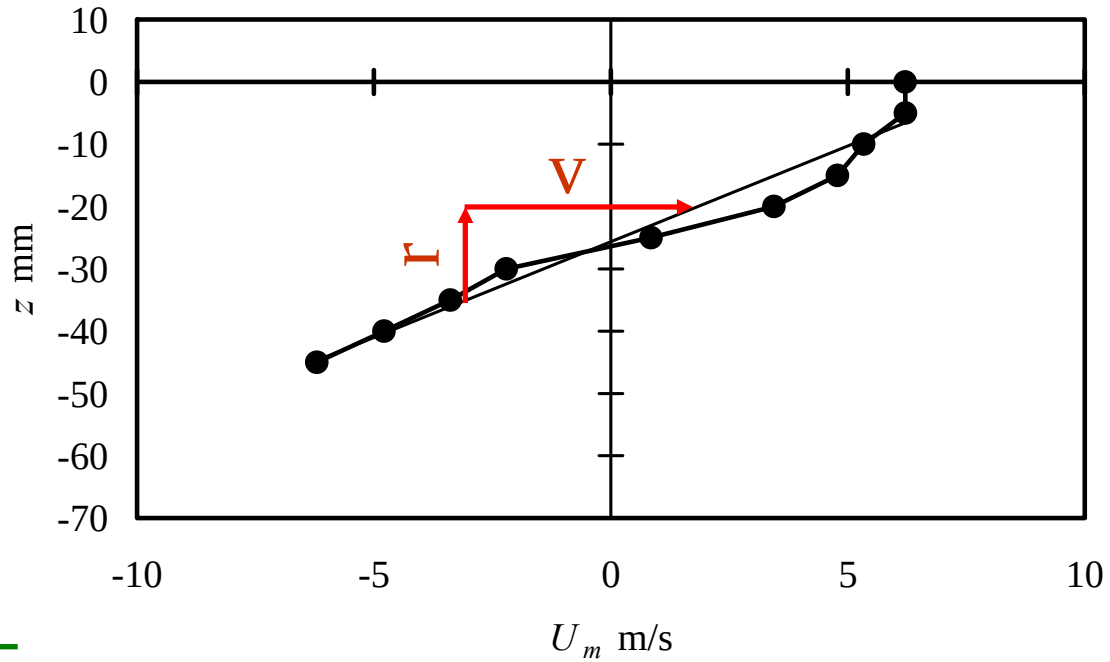

- Linier fitting of velocity distribution
- Estimate the angular rotation speed ω

$$\frac{\omega_{Tumble}}{\omega_{Shaft}} = TR$$

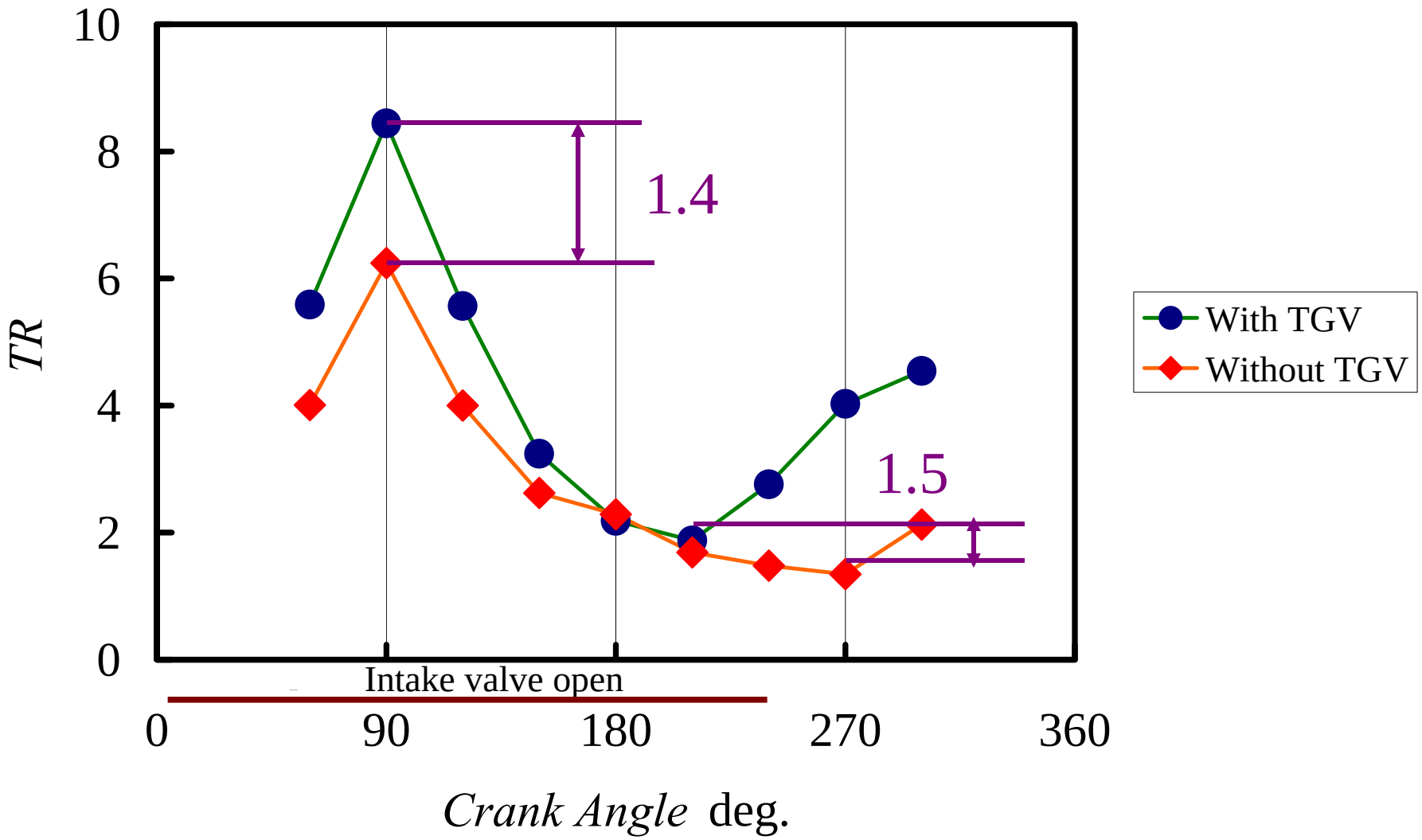

Tumble ratio

CONCLUSION

LDA measurements are performed in order to construct the database for verification of numerical simulation.

The effect of the tumble generation valve (TGV) is evaluated by velocity distributions. The concluding remarks are followings:

1. Velocity distributions in two-directions are obtained with each crank angle. The database can be used for verification of numerical simulations.
2. The effect of TGV is clarified by the experimental data.

More detailed results and turbulence characteristics are reported soon.

LDA Measurement of Gas Flow in a 4-stroke Motored Engine

Tomio OBOKATA, Tsuneaki ISHIMA and Hirohito YOKOTA
Graduate School of Mechanical Engineering, Gunma University
1-5-1 Tenjin, Kiryu 376-8515, JAPAN

An experimental study on in-cylinder flow measurement has been performed in order to make standard database for verifying numerical simulation. A laser Doppler anemometer (LDA) is applied to measure the velocities of vertical- and swirl-directions in the transparent sapphire cylinder of test engine made by Subaru. The time-series velocity data are readjusted by the ensemble averaged method using crank angle windows. Mean velocity and rms velocity are calculated with each crank angle. The tumble motion is evaluated by mean velocity map.

1. INTRODUCTION

For better thermal efficiency and less harmful exhaust gas, it is important to analyze and improve the combustion process in internal combustion engines. Current technology of the internal combustion engine like as gasoline direct injection system uses combination of spray and in-cylinder flow. Then, there are many experimental research works about the in-cylinder flow [1-4]. Although the experimental works are performed successfully, there is no common understanding for gas flow due to intermittent, highly turbulent and 3-dimensional complex flow field in actual engine. In this study area, numerical simulation is one of the important tools for obtaining the velocity fields. However, verification of the results of the numerical simulation has a lot of difficulties because of a lack of experimental data in good accuracy. The purpose of the present study is to prepare the standard database on the turbulent characteristics of in-cylinder flow velocity.

2. EXPERIMENTS

2.1 Test Engine

Table 1 shows the 4-stroke and single cylinder type. The bore and stroke is 96.9 mm x 74 mm. The shapes of combustion chamber and piston head are pent roof and flat shape, respectively. The cylinder is made by sapphire for optical access. The engine is mortared under 600 rpm in this report. The engine has tumble generation valve (TGV). The change in the velocity pattern with and without TGV is evaluated. Figure 1 shows the arrangement of experimental apparatus. The crank angle of the engine is monitored with a rotary encoder. All of the velocity information is analyzed by the ensemble averaged method in this report.

Table 1 Engine specifications.

Engine type	4-stroke, Single cylinder
Combustion chamber	Pentroof type
Bore × Stroke	96.9 mm×74 mm
Displacement	545.7 cc
Compression ratio	11.5
Intake valve opening	4 deg.
Intake valve closure	240 deg.
Exhaust valve opening	485 deg.
Exhaust valve closure	5 deg.

Table 2 LDA properties.

Wave length	632.8 nm
Beam separation	50 mm
Beam diameter	1.35 mm
Focal length	300 mm
Full beam cross angle	9.52 °
Calibration factor	3.81 m/s/MHz
Diameter of waist	179 μm
Measuring volume length	2.26 mm
Measuring volume width	179 μm
Shift frequency	10 MHz

2.2 Measurement setup and methods

The measurement has been carried out by using a laser Doppler anemometer (LDA). The LDA consists of He-Ne laser and burst spectrum analyzer (BSA, Dantec 57N20). Forward scattering mode is applied for better signal quality and data rate. Frequency shift which uses negative velocity measurement is 10 MHz. Table 2 shows detail property of the specifications of test engine. The engine is

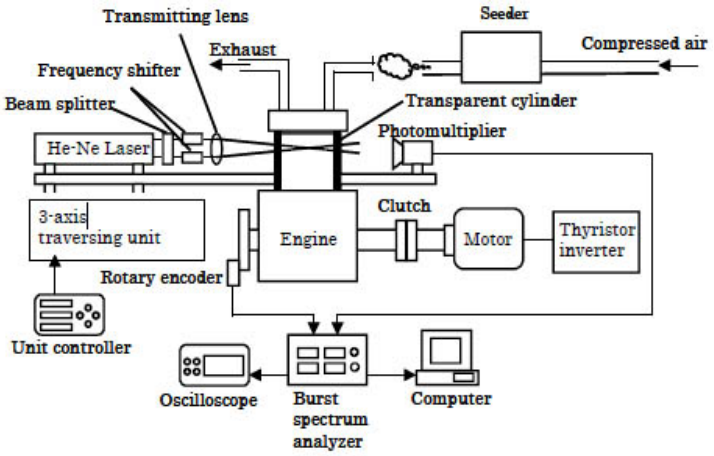

Fig. 1 Experimental setup.

LDA. The origin of the coordinate system is on center of the piston head at TDC. The coordinate system is shown in Figure 2 which is cylinder head view from the top side. The cylinder axis is z direction. B-B plane is on center line between intake and exhaust valves and is set to *x*-*z* plane. A-A plane is perpendicular to the B-B section and is set to *y*-*z* plane.

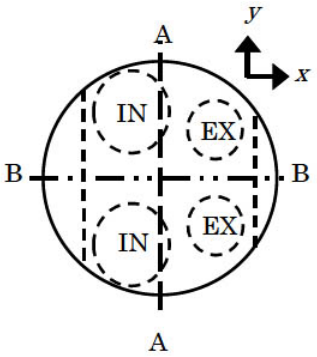

Fig. 2 Coordinate system.

Table 3 Tracer particles.

TiO_2 (KURONOS TITAN 2220)	
Mean particle size	0.4 μm
Density	4.0 g/cm^3
SiO_2 (Degussa AEROSIL R812)	
Mean particle size	7 nm
Density	2.2 g/cm^3

The velocities of cylinder axis and swirl directions on the A-A and B-B planes are measured. The measurement positions are each 5 mm in - 45 mm ≤ *y* ≤ 45 mm and - 65 mm ≤ z ≤ 7 mm of A-A plane, and - 45 mm ≤ *x* ≤ 45 mm and – 65 mm ≤ z ≤ -10 mm of B-B plane. 50000 samples are obtained at all of the measurement points. The LDA measurement needs tracer particles. In the study, Titanium dioxide (TiO2) of 0.4 μm in diameter is used and Silicone dioxide (SiO2) of 7 nm is added with 2 % of weight ratio. Properties of the particles are shown in Table 3.

3. RESULTS AND DISCUSSIONS

3.1 Velocities in tumble direction with and without TGV

Figure 3 shows the axial velocities measured at x, *y*, *z* = 0, 0, -10mm attached with TGV (a and b) or without TGV (c and d). Figure 3 (a) and (c) show the instantaneous axial velocity of *W* obtained within 100 rotation cycles. The ensemble averaged mean velocity of W_m and fluctuating intensity of w_{rms} are plotted at Figure 3 (b) and (d). There are no data durations in the figures because the incident laser beams are blocked by piston or intake valves in the cylinder.

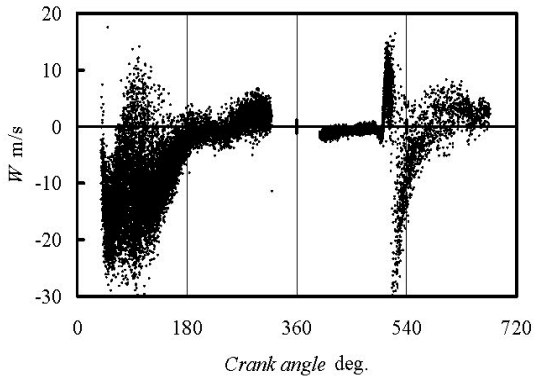

(a) Instantaneous velocities in many cycles with TGV

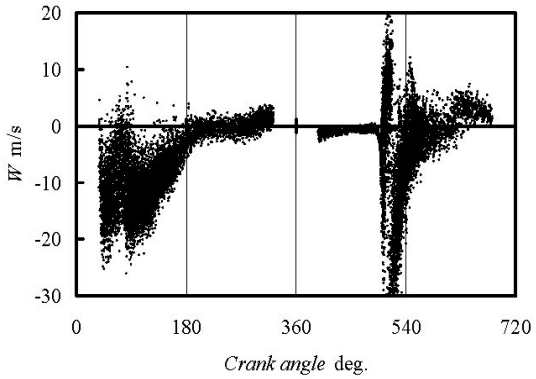

(c) Instantaneous velocities in many cycles without TGV

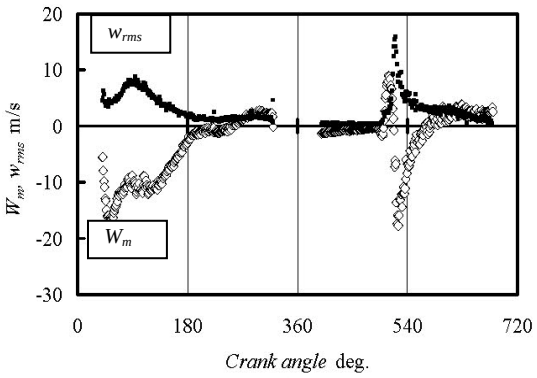

(b) Mean and fluctuating velocity with TGV

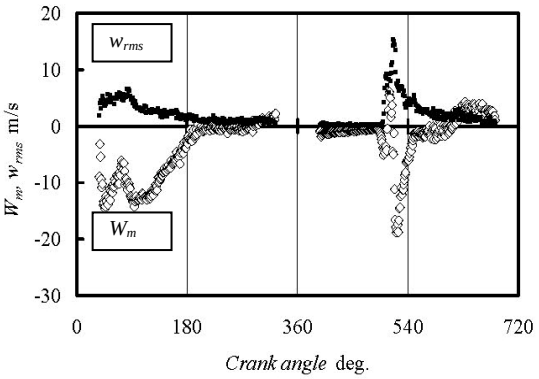

(d) Mean and fluctuating velocity without TGV

Fig. 3 Examples of axial velocity data measured by LDV with TGV or without TGV
(Engine speed: 600 rpm, Motoring, WOT)

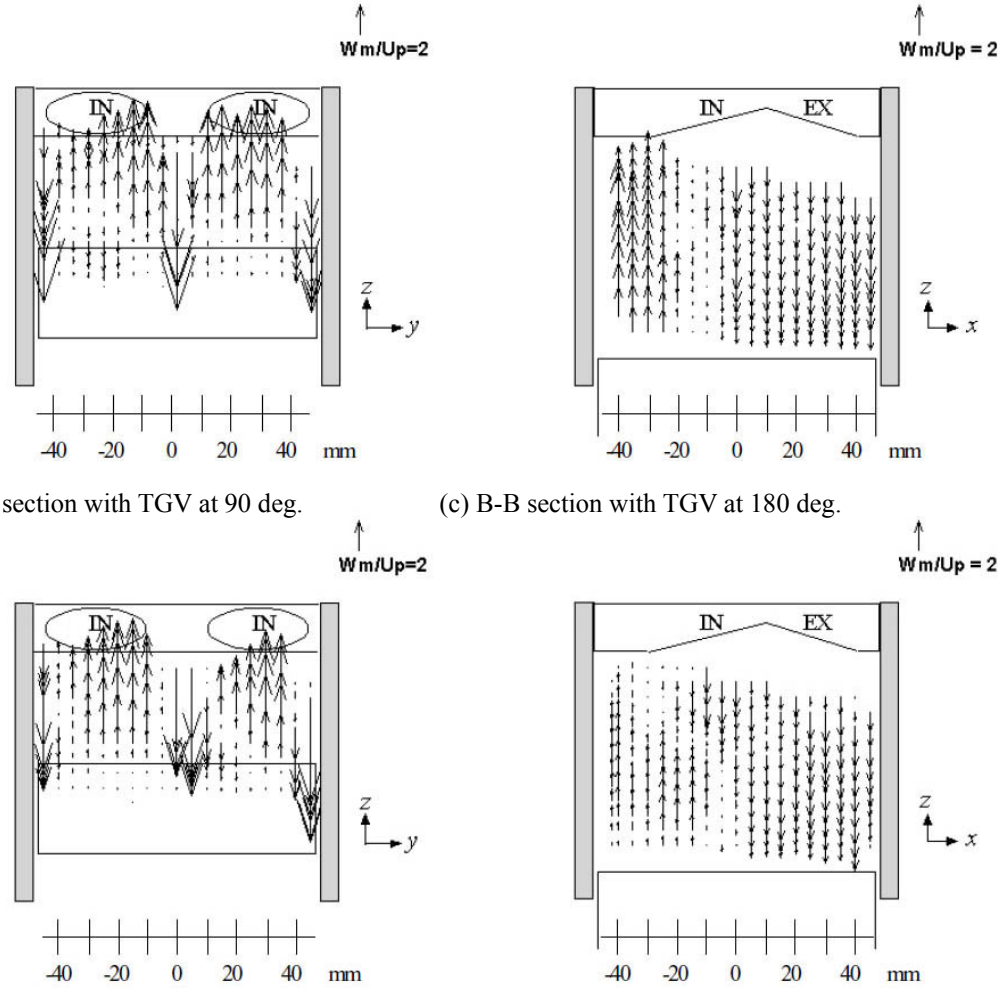

(a) A-A section with TGV at 90 deg.

(c) B-B section with TGV at 180 deg.

(b) A-A section without TGV at 90 deg.

(d) B-B section without TGV at 180 deg.

Fig. 4 Ensemble-averaged mean velocity distributions of W_m at vertical section
(Engine speed: 600 rpm, Motoring, WOT, at CA = 90 deg. and 180 deg.)

At the intake stroke, higher *W* velocities in minus direction are observed in "with TGV" case comparing with "without TGV" experiment. Same tendency is also shown in w_{rms} data.
Figure 4 shows velocity distributions of A-A and B-B sections at 90 and 180 degrees of crank angle. The figure indicated both flow fields of with and without TGV conditions. The velocities are normalized by the mean piston velocity of *Up* = 1.48 m/s which corresponds to the engine speed of 600 rpm. From the comparison between Figs. 4 (a) and (b), it shows similar velocity distribution. It seems that the TGV has less effect on the velocity in the plane. In detail, velocity magnitude with TGV is larger than that of without TGV case. Large velocity region can be observed at cylinder center line (y = 0 mm) and near the cylinder wall (y = ± 45 mm). There is reverse flow at the behind of intake valves. In the B-B section as shown in Figs. 3 (c) and (d), the TGV affects the velocities at intake valve side of B-B plane at 180 degree of crank angle. The results indicate the larger tumble motion at the with TGV condition.

3.2 Velocities in swirl direction with and without TGV

Figure 5 shows velocity distributions of z = -10 and -60 mm planes at 180 degree of crank angle. The velocities are measured in only A-A and B-B planes. The mean velocities of *Um* and *Vm* is normalized by mean piston speed of *Up* = 1.48 m/s under engine speed of 600 rpm. At *z* = - 10 mm, the velocity in *x* direction changes between with and without the TGV. When the TGV exists, the velocity in *x* direction becomes larger than that of without TGV condition. On the other hand, velocity in y direction has small changes with conditions. At *z* = - 60mm as shown in Figs. 4 (c) and (d), the velocity distributions are nearly equal to each other. The velocity magnitude with the TGV is larger than that of without the TGV case.

Combination on the velocity distributions in A-A plane at *z* = - 10 and - 60 mm provides the tumble motion. The results indicate that the TGV creates strong tumble motion. On the other hand, the TGV has less effect on the swirl motion.

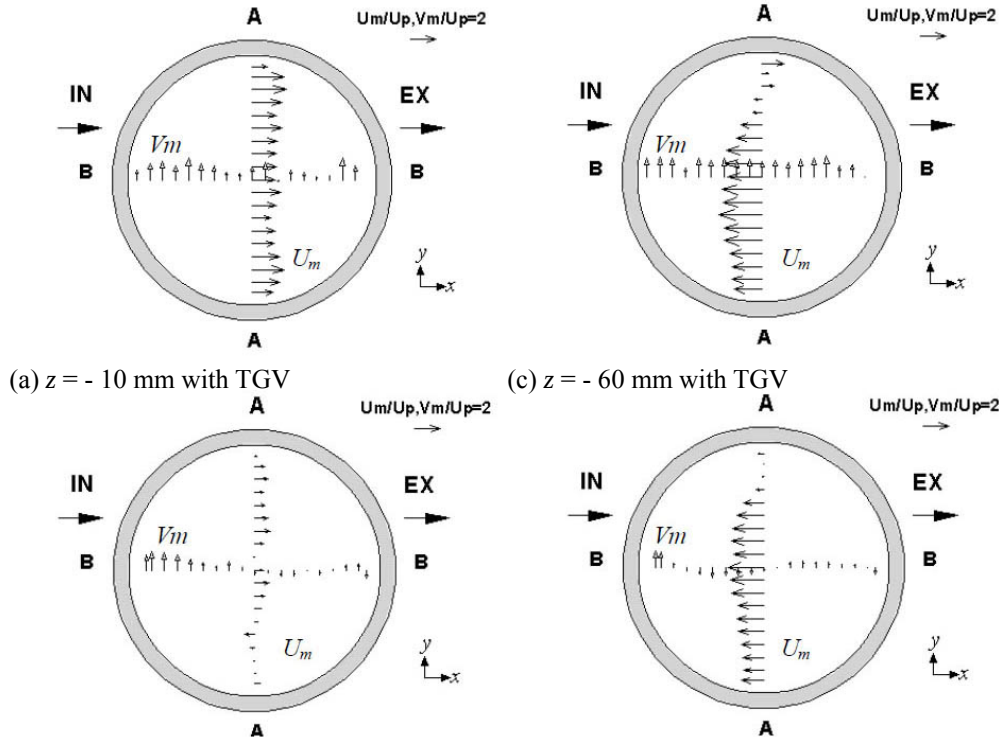

(a) z = - 10 mm with TGV (c) z = - 60 mm with TGV

(b) z = - 10 mm without TGV (d) z = - 60 mm without TGV

Fig. 5 Ensemble-averaged mean velocity distributions of U_m and V_m at transversal section (Engine speed: 600 rpm, Motoring, WOT, z = - 10, - 60 mm at CA = 180 deg.)

3.3 Tumble ratio

Figure 6 shows tumble ratio obtained from the axial velocity distribution as shown in Figure 4. Higher tumble ratio is observed in "with TGV" case in compression stroke.

4. CONCLUSION

LDA measurements are performed in order to construct the database for verification of numerical simulation. The effect of the tumble generation valve (TGV) is evaluated by velocity distributions. The concluding remarks are followings:

1. Velocity distributions in two-directions are obtained with each crank angle. The database can be used for verification of numerical simulations.
2. The effect of TGV is clarified by the experimental data.

More detailed results and turbulence characteristics are reported soon.

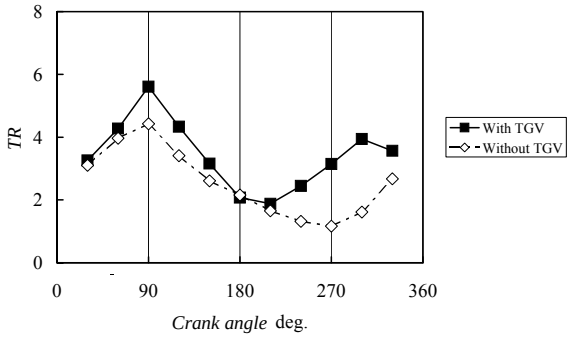

Fig. 6 Tumble ratio

REFERENCES

1) UEKI, H., ISHIDA, M. and EGAMI, H., Study on In-Cylinder Flow of Direct Injection Diesel Engine by LDV Measurements, Transactions of JSME, Series B, Vol.55 No.511(1989), pp.910-915 (in Japanese)
2) OBOKATA, T., HANADA, N., KUWAHARA, H. and KURABAYASHI, T., Measurement of Gas Velocity in a Combustion Chamber of a Small-Size, two-Stroke S.I. Engine by LDA, Transactions of JSME, Series B, Vol.54 No.505(1988), pp2687-2693 (in Japanese)
3) KANEKO, M., IKEDA, Y. and NAKAJIMA, T., Tumble Generator Valve (TGV) Control of In-cylinder Bulk Flow and Its Turbulence Near Spark Plug in SI Engine, SAE Paper, No.2001-01-1306 (2001)
4) MORIYOSHI, Y., KAMIMOTO, T. and YAGITA, M., Prediction of Cycle-to-Cycle Variation of In-cylinder Flow in a Motored Engine, SAE Paper No. 930066.

Subtask 1.4G:
INVESTIGATE COMBUSTION IN PREMIXED CHARGE SPARK/COMPRESSION IGNITION ENGINES

Analysis of Knocking by Measuring Local Gas Temperature Using Two-wire Thermocouple

Yasuo Moriyoshi, (Chiba University, Japan)

ABSTRACT - The phenomenon of autoignition is an important aspect of spark ignition engine knocks, hence reliable information on the relationship between the local gas temperature and the autoignition delay in a combustion chamber must be obtained to avoid knocks. However, the measurement of local gas temperature, especially near the wall where a knock occurs is difficult. Recently, several studies have been conducted by using laser techniques such as CARS. It has a high spatial resolution, but has been proven difficult to apply in the vicinity of the combustion chamber wall and requires special measurement skills. Meanwhile, a thermocouple is useful to measure local gas temperature even in the vicinity of wall. However, a conventional one-wire thermocouple is not adaptable to measure the in-cylinder gas temperature due to its slow response. The issue of response time can be overcome by adopting a two-wire thermocouple. The two-wire thermocouple is consisted of two fine wire thermocouples with different diameter hence it is possible to determine the time constant using the raw data from each thermocouple.

In this study, measurements such as local gas temperature inside a constant-volume combustion chamber, pressure and visualization were achieved with and without autoignition. Thereby, the relationship between the ignition delay and the gas temperature was clarified. This is a very important result for analyzing the knock phenomenon. As a result, negative temperature coefficient was found to mostly affect autoignition in this experimental condition. This technique was applied at more engine-like conditions, by developing a new rapid compression machine (RCM). The local gas temperature inside the combustion chamber under compression with and without combustion was measured to examine the heat loss and propagating local flame structure.

INTRODUCTION

In order to improve the thermal efficiency of spark ignition engines, control of knock is an important issue. Control of autoignition is a key technology for accomplishing low exhaust gas emissions and fuel economy by avoiding heavy knocks. Thereby, the study of autoignition of fuel-air mixture has been carried out by many researchers [1-6]. Recently, analyses of autoignition have been widely carried out theoretically using a chemical reaction codes such as "CHEMKIN" [7,8]. Experimental analysis is also achieved by some techniques such as visualization, chemical species measurement using LIF, and temperature measurement using CARS. Among them, the local gas temperature measurement is the most important factor for analyzing the autoignition although it has proven been very difficult.

In spark-ignition engines, the knock phenomenon has been examined as a subject of autoignition. Recently, a study of knocks has been conducted made using rapid compression machines (RCMs) or shock-tube [1-6]. In this manner, detailed knock phenomenon in a real engine should be analyzed under a condition where flame propagation exists during the autoignition induction period. On the other hand, the analysis using a real engine causes a difficulty to remove the effects of temporal changes in pressure and temperature by the piston movement.

Thereby, the objective of this study is to clarify the relationship between the local gas temperature and the autoignition delay by measuring the gas temperature using a two-wire thermocouple. At first, a knock phenomenon was realized in a constant-volume chamber as the first step where ignition was accomplished by a spark plug and the flame was initially propagated. Near instantaneous local gas temperature measurement has been required to investigate the knock phenomenon because the gas temperature in the unburned region greatly affects the chemical reactions and it is an indispensable factor to make quantitative comparisons with calculated results. It has been possible to do this using the CARS technique [9], however the accuracy, complexity of the setup and difficulty in obtaining measurements near the walls have been limiting factors. The authors introduced a two-wire thermocouple [10-12] that can attain a near instantaneous measurement of local gas temperature. At the same time, an endoscope was used to visualize the combustion process. By a combination of local temperature detection, visualization and pressure analysis, possible influencing factors on knock phenomenon were examined.

As a second step, experiments using RCMs were completed under engine-like conditions such as temporal variations of pressure, temperature and gas motion. Thereby, the design and construction of a RCM was carried out. The details of structure and the results of preliminary tests of local gas temperature measurement under compression with and without combustion are also reported to examine the heat loss from the wall and the propagating flame structure.

TWO-WIRE THERMOCOUPLE

The structure of the two-wire thermocouple is illustrated in Fig. 1. Relatively thin and thick thermocouples were closely set using four struts. Two wires of K-type (Chromel/Alumel) or R-type (Platinum and Platinum-Rhodium) with thicknesses between 25 and 100 μm were used to have a clearance of 0.1 mm between the two hot-junctions, corresponding to the thickness of the relatively thick thermocouple. This standard for the clearance length was examined in the authors' paper [12].

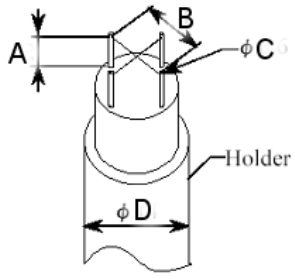

Fig. 1 Structure of two-wire thermocouple

Table 1 Specifications of thermocouple

	K-type	R-type
Strut length, A	10 mm	2.5 /4 /6 mm
Wire length, B	8 mm	3.5 mm
Strut diameter, C	0.6 mm	0.65 mm
Sensor diameter, D	14 mm	5 mm

Thinner thermocouple wires have shorter time delays. However, those wires with a thickness of less than 50 μm will eventually burn during repeated combustion events. In the short term, a K-type thermocouple with a thickness of 25 μm can be adopted, although it will burns out under several runs of combustion. R-type can withstand longer duration. Each thermocouple was made by using a percussion welding to make a hot-junction. Only inspected thermocouples were used that have no deviation of wire centers within 10% in diameter and the same size of hot-junction within 10% deviation as that of wire.

Basic equation of thermocouple is Eq. 1 assuming first order lag, where T_g, T and τ are gas temperature, hot-junction temperature and the time constant, respectively.

$$T_g = T + \tau\,(\mathrm{d}T/\mathrm{d}t) \qquad (1)$$

An unknown quantity is only τ in the righthand-side of Eq. 1 and there are several methods to estimate that. Two wires were used as τ can be estimated directly. The system works using the following principle two sensors with two differing thermal inertia are adopted to measure a known temperature, while the corresponding time constants are adjusted to correct for thermal inertia. The details such as the response time under several conditions are available in other papers [10-12], where one can find a method for obtaining the near instantaneous gas temperature in the end-gas region accompanying flame propagation. Here, the theory is briefly introduced.

Basic equations for estimating the gas temperature are shown in Eq. 2, where the subscripts 1 and 2 denote the thin and thick thermocouples respectively.

$$T_{g1} = T_1 + \tau_1 \frac{dT_1}{dt},\ T_{g2} = T_2 + \tau_2 \frac{dT_2}{dt} \qquad (2)$$

Although T_{g1} and T_{g2} should be identical ideally, the difference between T_{g1} and T_{g2} exists actually. Thus in this concept, time constants, τ_1 and τ_2, are determined by minimizing the value of e using the least square method, as shown in Eq. 3.

$$e = \frac{1}{N}\sum_{i=1}^{N}\left(T_{g1}^{i} - T_{g2}^{i}\right)^2 \qquad (3)$$

where N is the number of samples for each thermocouple.

EXPERIMENTAL APPARATUS USING COMBUSTION CHAMBER

Combustion Chamber and Visualized Area

Figure 2 shows the schematic of a combustion chamber employed in this study. The chamber is pancake shaped in ϕ120 x 20 mm height (volume 226 cc) and equipped with electric heaters in upper and lower parts and wall periphery to control initial wall and gas temperatures up to 600 K. To prevent inhomogeneity of wall temperature distribution, the

wall was once heated over the set temperature and naturally cooled to the set temperature. The temperature distribution around the chamber was confirmed to be within one degree. Moreover, in order to cause autoignition in the end-part of the chamber, a spark plug is positioned shifted 45 mm from the center of the chamber. The thermocouples of K-type indicated in Table 1 are located at two positions of at the center of chamber (CNT) and at the end-part (END) as illustrated in Fig. 3. The figure also designates settings of sensors viewed from the top of the chamber. The CNT thermocouple is located 45 mm left of the spark plug while the END thermocouple is 97 mm left of the spark plug and 8 mm left from the wall. The position in height is fixed just at the middle of the chamber.

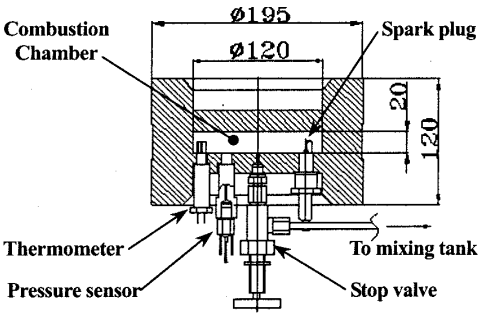

Fig. 2 Schematic of combustion vessel

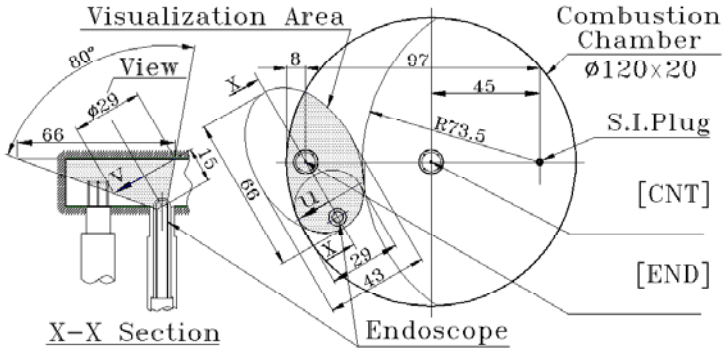

Fig. 3 Thermometer locations and visualized area through endoscope

In this study, it is necessary to keep the wall and gas temperatures around the low-temperature reaction region (~600 K) to examine the effect of the negative temperature coefficient (NTC) region [3], where the ignition delay becomes short as the gas temperature increases. This prevents from setting a large optical window in the wall. Instead, an air-cooled endoscope (AVL MO0117, ϕ4, Hopkins linear lenses) was used with a wide field-view angle of 80 deg. Also, a water-cooled piezo-type pressure transducer (Kistler 601B) was installed near the spark plug.

The initial temperature and pressure of charged mixture can be controlled by adjusting both the wall temperature and the charging pressure. Followed by mixture charging, the spark ignition was made. As the flame propagation inside the chamber causes a compression of unburned gas, leading to increases in pressure and temperature of end-gas, the initial gas temperature and pressure were controlled to bring with a scheduled temperature of the end-gas. Preliminary experiments were carried out to achieve an autoignition within the end-gas and the experimental conditions are listed in Table 2.

Table 2. Experimental conditions

Fuel	n-Pentane
Oxidizer	O_2
Dilution Gas	Ar
O2 / Ar (vol. ratio)	40%
Equivalence ratio	0.35
Mixture State	Pre-mixed charge
Wall Temperature	307,323,373,423,443,463,473, 483,493,503,513,518,[K]
Charge Pressure	0.3 [MPa]

All experiments were carried out with an equivalence ratio of 0.35. By adopting Ar gas as a diluent rather than N_2, the gas specific heat was decreased, hence raising the maximum achievable gas temperature. In this study, the charge pressure was fixed, hence the mass of charged mixture decreased with increasing the wall temperature.

EXPERIMENTAL METHOD

The prescribed mixture was prepared using a tank with a rotating fan, where fuel, oxygen and diluent were mixed and well stirred for three hours using a rotating fan. The tank was heated to enhance the fuel evaporation and prevent the formation of condensation. The wall temperature of the combustion chamber was controlled and the chamber was evacuated to charge the mixture up to the prescribed pressure. A spark was ignited to induce a flame which propagated across the chamber and compressed the unburned gas in the end-gas region. The temporal variations of pressure and outputs from two thermometers were recorded with a digital oscilloscope. The digitized data were transferred to a PC. By using the recorded pressure, the bulk temperature and apparent rate of heat release were estimated. The repeatability was confirmed by completing the same experiment three times at each condition.

RAPID COMPRESSION MACHINE

Rapid Compression Machines (RCMs) are often adopted to simulate a single engine combustion event. This enables easy measurements of physical properties by using sensors and optical visualization techniques. In this study, the system at Kyusyu University [13] was employed for the reasons discussed in the next section.

An outline of the RCM is shown in Fig. 4. The RCM comprises of five main units, pressure reservoir, driving, cam, compression and combustion units. For operation, firstly, compressed air was charged in the reservoir tank. Secondly, a barrier membrane was smashed by a sharp pin operated by a solenoid. Thirdly, a piston in the driving unit was driven by a compressed air and the cam moves quickly. And then, another piston in compression was driven by a rod which contacted the cam surface to realize a rapid compression of the combustion chamber.

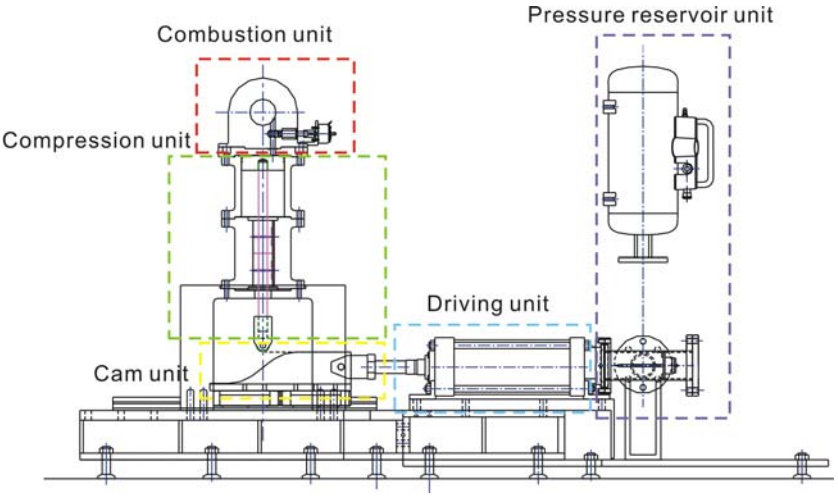

Fig. 4 Outline of Rapid compression machine

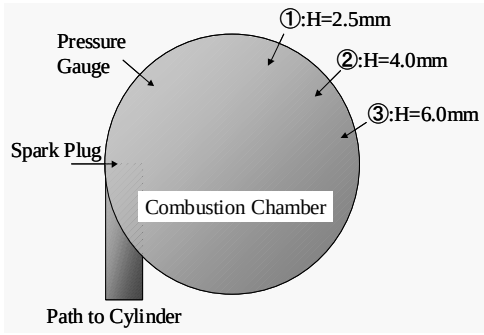

Fig. 5 Combustion chamber profile

Table 3 Specifications of RCM

Profile	Pancake (ϕ80 x t16 mm)
Volume	in-chamber: 80.4 cc out-of-chamber: 36.8 cc
Compression ratio	11.5

The specifications of the combustion chamber are listed in Table 3. The combustion chamber is of a pancake shape with a volume of 80.4 cc. In this machine, in order to visualize the whole space of the chamber, a pancake shaped chamber with two quartz windows was adopted. Thereby, some dead volume such as the connecting passage was caused. Figure 5 shows schematics of the chamber. As the compressed gas enters the combustion chamber through the connecting passage shifted to the left side of the chamber, a swirl flow is generated. As the spark plug is located near the passage port, flame propagates in the chamber on the swirl flow. The piston position of combustion chamber is measured using an optical laser displacement meter (OMRON, ZX-LD300). The gas pressure inside the chamber was detected using a piezoelectric sensor. The local gas temperature inside the chamber was measured using two two-wire thermocouples including near wall location as indicated in Fig. 5. Fuel and air were mixed using a tank with a heater. The mixture was supplied to the combustion chamber. The combustion period including compression period was typically less than 100 ms.

In this duration, sequential operations such as the breaking of the barrier membrane, onset of spark and closing of the connecting passage between combustion chamber and mixture tank were made.

EXPERIMENTAL RESULTS USING A CONSTANT-VOLUME CHAMBER

Effect of Initial Wall Temperature on Pressure Wave

Experiments were performed by raising the wall temperature to those indicated in Fig. 6(a). The period of combustion apparently decreased. The reference time of zero in Fig. 6 is the timing of spark ignition. The combustion noise is indistinct sound, but it changes to an intense sound with raising the wall temperature. When the initial wall temperature was set at between 503 and 518 K, the pressure oscillation was observed with a frequency of 3.9 kHz, corresponding to the nearly predicted knock frequency using the estimated sound velocity in this experimental condition. When the oscillation occurred, the pressure drop after the peak became large due to an increase in heat loss. This is evidence of knock inside the chamber. Thus, knock was realized in a constant-volume chamber with flame propagation without piston compression. However, increasing the initial wall temperature above 518 K caused autoignition before spark-ignition.

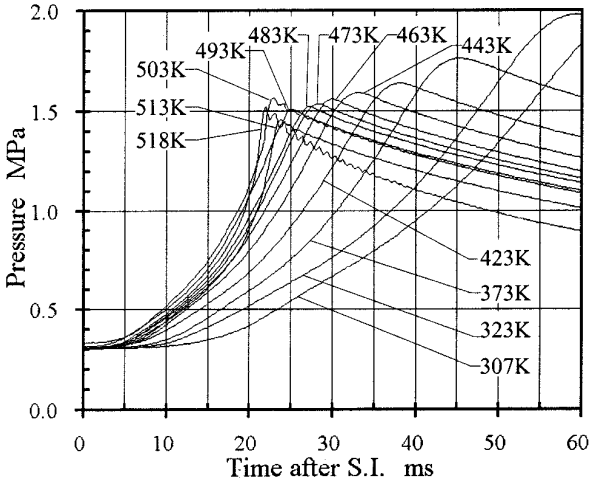

Fig. 6(a) Pressure histories in various wall temperatures

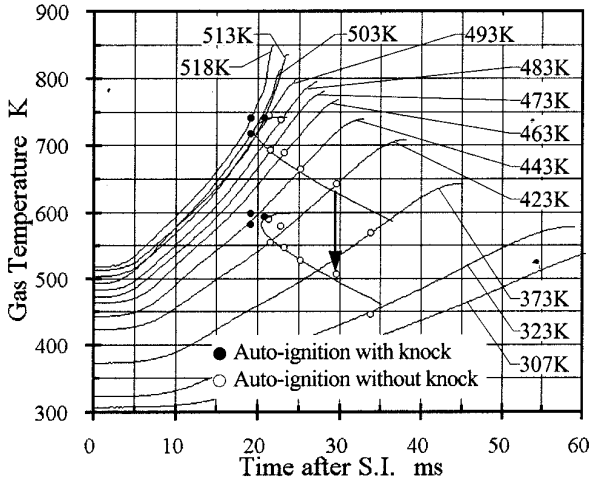

Fig. 6(b) Unburned gas temperature history in various wall temperatures

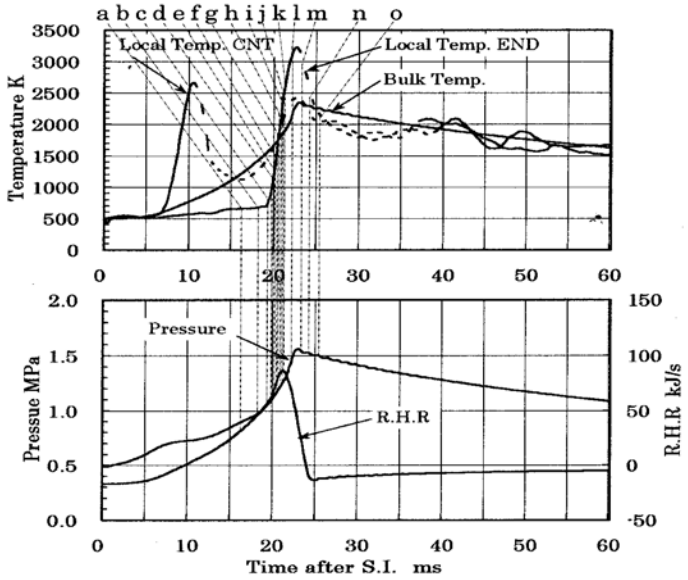

Fig. 7 Local gas temperature and pressure histories in non-knock condition (Wall Temp. 503 K)

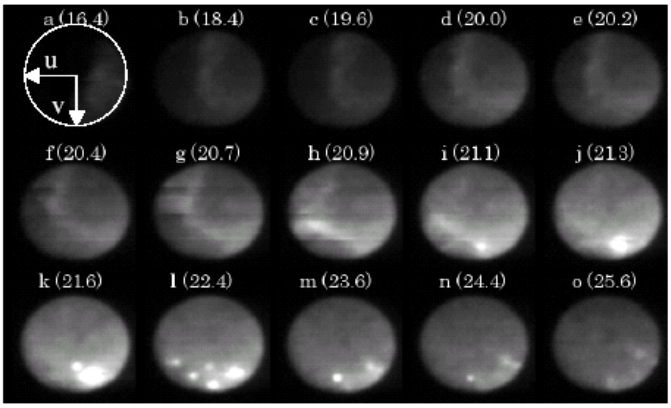

Fig. 8 High-speed photographs through endoscope observing in the end gas region (Wall Temp. 503 K)

Here, the bulk temperature can be almost presumed using a pressure value assuming an adiabatic compression because the compression by flame propagation is quick.

$$T_{bulk} = T_0 (P_0 / P)^{1/(\kappa-1)} \qquad (4)$$

The specific heat ratio, κ was set at 1.45. The estimated bulk temperature is indicated in Fig. 6(b). The effect of the initial wall temperature on pressure and bulk gas temperature can be observed in Figs. 6(a) and (b).

Observation in Knock Conditions

Figure 7 shows the results of pressure and temperature at a condition (wall temperature at 503 K) with knocks. The estimated local temperatures at CNT and END are indicated in the upper figure. The measured local temperature accuracy after the flame passes by may become deteriorated as the gas velocity becomes small. The authors examined the effect of ambient gas velocity and density on the estimated temperature using a two-wire thermocouple [12]. Because a decrease in the gas velocity or density make the heat transfer less, the estimated temperature would be underestimated. Thereby, some part of the measured data was drawn in broken lines where the accuracy was estimated to be lower. The pressure, bulk temperature and rate of heat release are shown in the lower figure. High-speed video images (8bit, 256x256 resolution, 4500 fps, with I.I. gated in 100 μs) are shown in Fig. 8. The image quality is not good as an image-intensifier was employed. The view field of the endoscope was designated in Fig. 3 (X-X section). In each frame, the symbol (‘a’ to ‘o’) indicates the corresponding temperature and pressure in Fig. 7. Also, the number in parentheses indicates the time after spark timing in ms.

The local temperature at END sharply rose at 19.6 ms ‘c’, leading to a rapid increase from 700 to 3240 K. Pressure oscillation that is a feature of knocks was

observed and the first appearance of the peak coincides with that in temperature signal at 23 ms. This means that autoignition occurred in the end-gas region and that it was detected by both pressure and temperature. The images are different from those in Fig. 8. Before the flame propagation was completed, strong luminescence was observed from 20.7 ms. Rapid reactions seemed to occur immediately and the peak of heat release indicated a high value of 87 kJ/s.

In previous studies, "hot spots" were observed in the unburned region using LIF measurement of CH_2O [14], leading to the chance of autoignition before knock initiates. In this study, identification of CH_2O could not be made, but highly illuminated spots in images ('j', 'k' and 'l') were probably equivalent to the "hot spot" in [14]. These spots disappeared at 25.6 ms as soon as the heat release was completed.

Relationships Between Unburned Gas Temperature and the Onset of Autoignition

The initiation of autoignition was defined as the time at which the local temperature was observed to increase. The relationship between the unburned gas temperatures estimated by pressure and the initiation time of autoignition were plotted on the graph of Fig. 6(b). Black circles indicate results with knocks while white ones do without knocks. When increasing the wall temperature, the initiation timing of autoignition was once advanced, but then retarded. This shows that the temperature at the initiation time of autoignition has an upper limit. That is reasonable because other experimental or theoretical results showed that hot flame appeared at almost the same temperature [15]. Regarding the temperature at the initiation time of autoignition, the definition in this study is different from other results using RCMs or shock-tube as autoignition occurs during compression accompanying with flame propagation in this study. Thereby, a mean gas temperature from the spark-ignition timing to the initiation of autoignition was estimated by integrating the near instantaneous temperature along the time and then, dividing the value by the past time. Here, it might not be appropriate to use this "mean gas temperature" because chemical reactions are non-linear but it is possible to examine the qualitative tendency. As a result, the mean gas temperature was almost 150 K less than that of the near instantaneous temperature at autoignition as shown in Fig. 6(b) with an arrow. The tendency between the two was found to be almost the same.

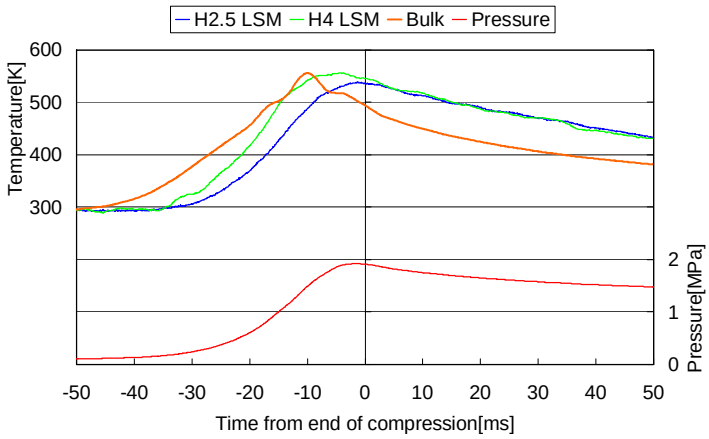

Fig. 9 Temporal variations of local and bulk temperatures and pressure without combustion

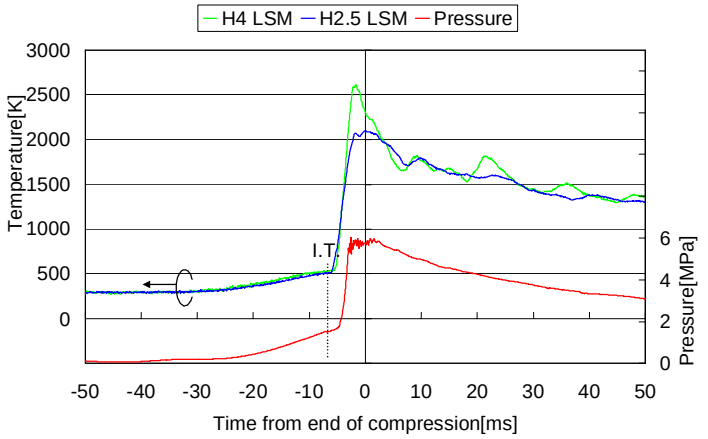

Fig. 10 Temporal variations of local temperature and pressure with strong knock (I.T. at -8 ms)

RESULTS USING RCM

At first, rapid compression was made without combustion in the previous study to check the validity of the two-wire thermocouple. Local gas temperature measurements were carried out at two locations 2.5 and 4 mm left from the wall using R-type thermocouple as indicated in Fig. 5. The results are indicated in Fig. 9. Compensated temperatures by using the least square method and bulk temperature from pressure data are plotted in the figure. As the time of zero means when the compression was completed (TDC), the compression was started around 50 ms before. The timing of maximum pressure was a little ahead of TDC because heat loss near TDC was large due to a large dead volume. The peak of bulk temperature was much ahead of TDC due to the same reason. During -50 to -35 ms, the bulk temperature showed a slight increase, but compensated local temperatures did not show an increase. This was due to a heat loss through the struts, supporting the thermocouple. Around -15 ms, the local gas temperature and the bulk temperature corresponded to each other. Before TDC, the local temperature 4 mm left from the wall showed a higher temperature than of 2.5 mm left because the heat loss was enhanced with decreasing the distance to the wall. However, after TDC, both temperatures were almost the same, while the bulk temperature was lower as a larger heat loss was caused in dead volume region where surface volume ratio was large.

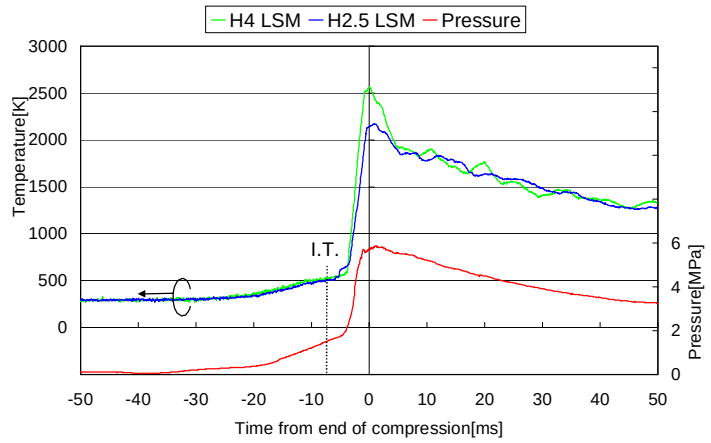

Fig. 11 Temporal variations of local temperature and pressure with weak knock (I.T. at -8 ms)

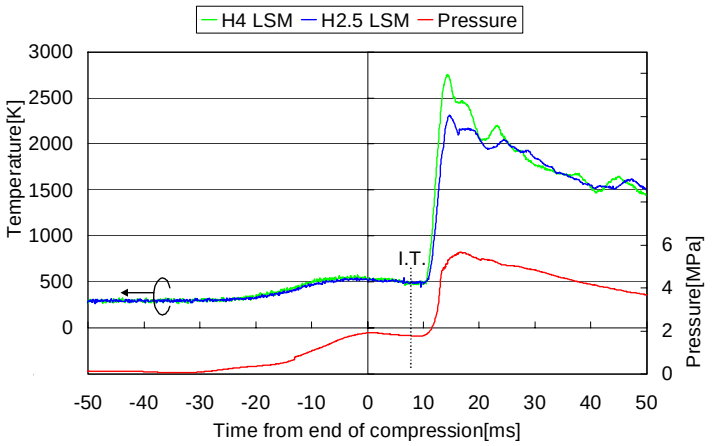

Fig. 12 Temporal variations of local temperature and pressure without knock (I.T. at 8 ms)

Following results were about combustion in stoichiometric with artificial air (N_2 : O_2 = 85 :15 in volume) condition using propane-air mixture. At this condition with the ignition timing of 8 ms before TDC, relatively strong or weak knocks occured. Each typical data are shown in Figs. 10 and 11, respectively. Comparing the two cases, the ignition delay (time from ignition to pressure rising) was shorter in a strong knock condition. The pressure gradient was also steeper. However, the temperature gradient was almost similar between the two as the flame propagation structure was not changed. The maximum temperature was around 2600 K, corresponding to the calculated adiabatic flame temperature. Moreover, the decrease in temperature and pressure due to heat loss was larger in strong knock condition as knock enhanced heat transfer to the wall. At this moment, the effect of NTC region cannot be discussed, since more results such as visualization would be taken in the near future.

Figure 12 shows the result with retarded ignition timing at 8 ms. In this case, as ignition was made so late after TDC while pressure decreasing, a knock was not observed. Although the pressure gradient was not so steep as previous cases, local temperature traces were similar to the previous ones. This means that local flame structure due to flame propagation was not changed. The local temperature at 2.5 mm was lower than of 4 mm as well as previous cases, but the temperature difference between the two was not large compared to the previous cases because the heat transfer to the wall is decreased due to without knocking and decay of swirl flow.

CONCLUSIONS

1. In order to measure near instantaneous local gas temperature inside a combustion chamber, two-wire thermocouple was developed. Using this sensor, local gas temperature near the wall (8 mm left) was measured under with knock and without knock conditions to examine the effect of negative temperature coefficient on the onset of autoignition.

2. By controlling the initial wall temperature of a constant-volume chamber at between 307 and 518 K, combustion of n-pentane, oxygen, and argon mixture was examined. Autoignition was detected at the end of combustion period with initial wall temperature at between 373 and 518 K. The onset of autoignition did not always lead to knock as some additional conditions were required. There found a relationship similar to “negative temperature coefficient” between the initiation times of autoignition and mean gas temperature when the mean gas temperature was between 580 and 600 K.

3. As the next step, combustion tests under engine-like condition such as the temporal variations of pressure, temperature and gas motion during the compression stroke were attained by using a RCM. Local gas temperature was measured under knock and non-knock conditions. As a result, information on the heat loss and propagating flame structure was found.

REFERENCES

(1) Halstead, M. P., Kirsch, L. J., Prothero, A., and Quinn, C. P., Proc. Roy. Soc. London ,A346 (1975), 515.
(2) Takahashi, H., Ohta, Y. Kinoshita, K., Trans.Jpn.Soc. Mech.Eng,Vol.48B, No.432 (1982), 1577.
(3) Ohta, Y. Furutani, M., Polish Academy of Sciences, vol.11, No.1-2 (1991) 43.

(4) Stiebels, B., Schreiber M. Sadat A.S., Development of a New Measurement Technique for the Investigation of End-Gas Autoignition and Engine Knock, SAE Paper No.960827
(5) Hu H. Keck J., Autoignition of Adiabatically Compressed Combustible Gas Mixtures, SAE Paper No.872110
(6) Senda, J. Fujimoto H.,Trans. of the JSAE, Vol.29, No.3 (1998), 11.
(7) Noel, L., Maroteaux, F., Numerical Study of HCCI Combustion in Diesel Engines Using Reduced Chemical Kinetics of N-Heptane With Multidimensional CFD Code, SAE Paper No. 2004-01-1909
(8) Iida, N., Yamasaki, Y., Sato, S., Kumano, K. Kojima, Y., Study on Auto-Ignition and Combustion Mechanism of Hcci Engine, SAE Paper No. 2004-32-0095
(9) Grandin, B, Denbratt I., The Effect of Knock on the Heat Transfer in An SI Engine: Thermal Boundary Layer Investigation Using Cars Temperature Measurements and Heat Flux Measurements, SAE Paper No. 2000-01-2831
(10) Cambray, P., Measuring thermocouple time constants : A new method ,Combust. Sci. and Tech., 45 (1986), 221.
(11) Tagawa, M., Okuda, M., Ohta, Y., Two-wire Thermocouple for Fluctuating Temperature Measurements in Combustion, Trans. Jpn. Soc. Mech. Eng, Vol.62B, No.598 (1986) 2506.
(12) Kobayashi, S., Moriyoshi, Y., Enomoto, Y., Auto-ignition of Premixed Mixture Using a Constant Volume Vessel, Prepr. of 17th Sympo. of the Int. Comb. Eng. (2002), 89.
(13) Murase, E., Performance of Pulsed Combustion Jet in a Rapid Compression Machine, Archivum Combustionis Vol.15, No.3-4 (1996) pp.173-185
(14) Westbrook, C.K., Kinetic modeling of hydrocarbon autoignition at low and intermediate temperature in a rapid compression machine,3rd Workshop on Modeling of Chemical Reaction Systems (1996).
(15) Choi, S., Moriyoshi, Y., Measurement of Local Gas Temperature inside a Combustion Chamber Using a Two-Wired Thermo-couple, JSAE No. 20055451